

PRELIMINARY DETECTION OF GEOTHERMAL MANIFESTATION POTENTIAL USING MICROWAVE SATELLITE REMOTE SENSING

Atriyon Julzarika and Udhi Catur Nugroho

Remote Sensing Applications Center

Indonesian National Institute of Aeronautics and Space (LAPAN)

E-Mail: verbhakov@yahoo.com and atriyon.julzarika@lapan.go.id

Received: 29 October 2017; Revised: 4 January 2019; Approved: 4 January 2019

Abstract. The satellite technology has developed significantly. The sensors of remote sensing satellites are in the form of optical, Microwave, and LIDAR. These sensors can be used for energy and mineral resources applications. The example of those applications are height model and the potential of geothermal manifestation detection. This study aims to detect the potential of geothermal manifestation using remote sensing. The study area is the Northern of the Inverse Arc of Sulawesi. The method used is remote sensing approach for its preliminary detection with 4 steps as follow (a) mining land identification, (b) geological parameter extraction, (c) preparation of standardized spatial data, and (d) geothermal manifestation. Mining lands identification is using Vegetation Index Differencing method. Geological parameters include structural geology, height model, and gravity model. The integration method is used for height model. The height model integration use ALOS PALSAR data, Icesat/GLAS, SRTM, and X SAR. Structural geology use dip and strike method. Gravity model use physical geodesy approach. Preparation of standardized spatial data with re-classed and analyzed using Geographic Information System between each geological parameter, whereas physical geodesy methods are used for geothermal manifestation detection. Geothermal manifestation using physical geodesy approach in Barthelmes method. Grace and GOCE data are used for gravity model. The geothermal manifestation detected from any parameter is analyzed by using geographic information system method. The result of this study is 10 area of geothermal manifestation potential. The accuracy test of this research is 87.5 % in 1.96 σ . This research can be done efficiently and cost-effectively in the process. The results can be used for various geological and mining applications.

Keywords: *The Northern of Inverse Arc of Sulawesi, geothermal manifestation, remote sensing, gravity model*

1 INTRODUCTION

Some of the survey and mapping of the potential of energy and minerals use various types of technology, one of which is remote sensing (KESDM, 1999). This remote sensing can be terrestrial, aerial, and space (satellite). The sensors that can be used in remote sensing are optics, microwaves, lasers, and sonar. Optical sensors use cameras with different types of visible, infra-red, and thermal bands.

Radar is an active microwave sensor. As the name implies, the radar

is developed as a way of using radio waves to detect the existence of an object and determine the distance (position). The process involves the transmission of short bursts or pulses of microwave power in the desired direction and recording its strength, as well as the origin of earthquakes or reflections received from objects in the field system of view. Most of the airborne sensing remote radar is performed with a system that uses an antenna mounted on the underside of the aircraft and is directed sideways.

This system is called Side Looking Radar (SLR) or Side Looking Airborne Radar (SLAR). The microwave image has a distinct advantage over the tropics, given its unclouded nature.

The microprocessor sensor has two distinct features that characterize microwave power, viewed from a remote sensing angle. In an example, microwaves can penetrate the atmosphere in varying circumstances, depending on the wavelength and reflections used and the micro-emissions from the material on the face of the earth are not directly related to the pair on the visible or thermal spectrum. The operation of this system is almost the same as the thermal radiometer (Zhou *et al.*, 2013). The theory of black body radiation is central to the conceptual understanding of passive microwave sensing, but passive microwave sensors emphasize the use of antennas rather than detection elements. Microwave signals generally consist of a number of source components that are partially transmitted, partially reflected, and partly transmitted.

Remote sensing data can be used

for preliminary surveys on potential energy and mineral resource identification applications (Youssef *et al.*, 2012). Remote sensing data will make time-efficient, cost-effective processes accelerate the analysis process in the preliminary survey (Julzarika *et al.*, 2018). In general, the process of identifying potential energy and mineral resources from remote sensing data consists of two types, namely minimal vegetation surfaces and many vegetation surfaces. On the minimal vegetation surface area, mineral resources potential can be identified with optical data, while on the area with many vegetation surfaces, mineral resources potential can be identified using microwave data, see Figure 1-1. According to EORC-JAXA (2018), remote sensing data are divided into two types of sensors, namely optical sensors and microwaves. Optical sensors consist of passive sensors (high resolution, global imaging, and spectral) and active sensors (LIDAR). The microwave sensor consists of a passive sensor (microwave radiometer) and an active sensor (SAR and Altimeter Scatterometer), see Figure 1-2.

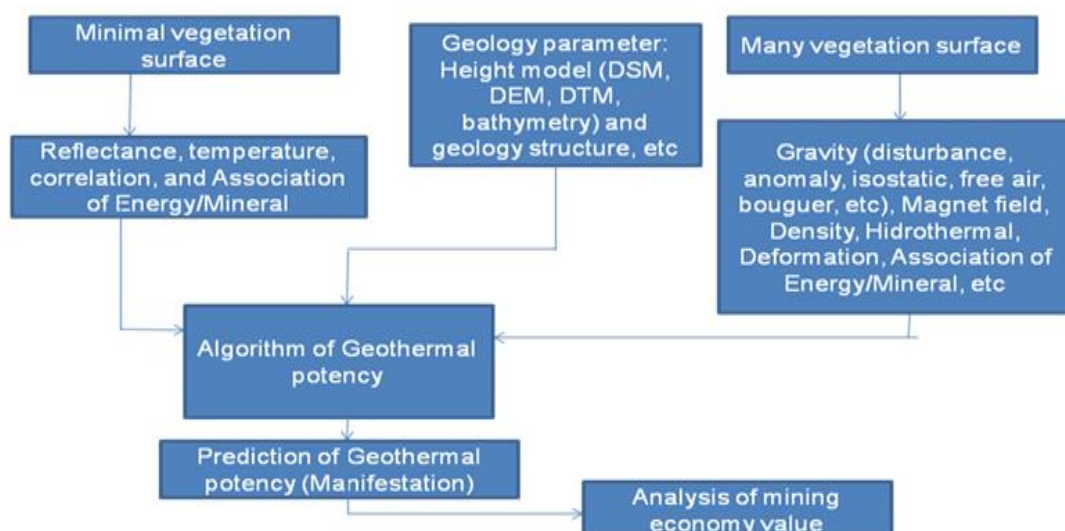


Figure 1-1: Different patterns of identification of energy mineral resources potential using remote sensing data (Julzarika and Anggraini, 2017)

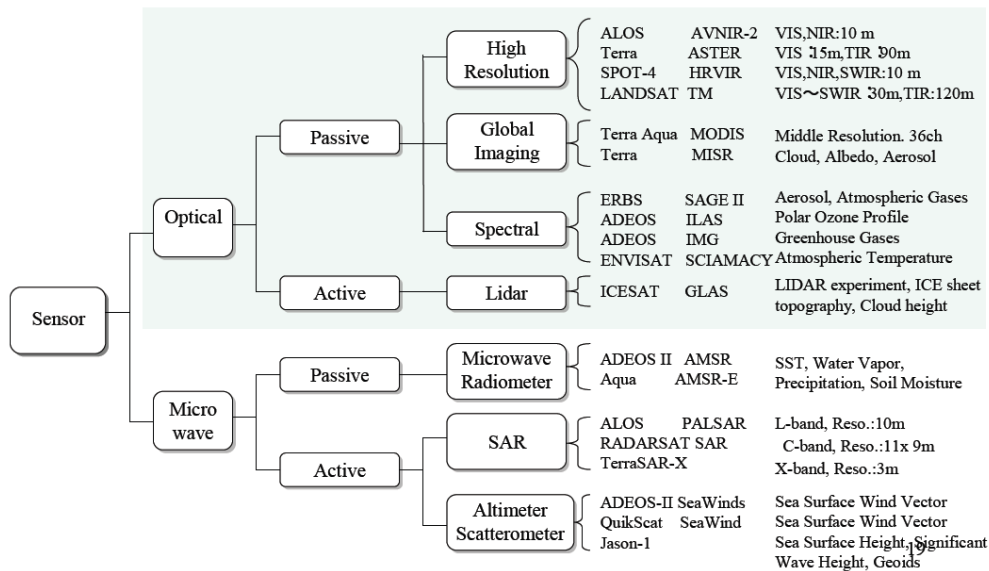


Figure 1-2: Distribution of remote sensing data types based on sensors (EORC JAXA, 2018)

Remote sensing data can also be used for height model extraction, ie. Digital Surface Model (DSM), Digital Elevation Model (DEM), and Digital Terrain Model (DTM). The method of DSM extraction commonly used is stereo. While the method of DSM extraction on microwave data is stereo SAR and Interferometry SAR (Jin *et al.*, 2014).

Geothermal is one of the potential energy that is available freely in the nature. This energy is rarely used in Indonesia. Geothermal can be used as a source of electrical energy. Remote sensing can be used for preliminary surveys to detect geothermal potential. The purpose of this paper is to detect the potential of geothermal manifestation using remote sensing.

2 MATERIALS AND METHODOLOGY

The research is located in the Northern of Inverse Arc of Sulawesi. This area is one of the rings of volcanoes that pass through Indonesia. This region is located near the Pacific plate, the Eurasian plate, and the Philippine Plate. The data used are data from Grace, GOCE, X SAR, SRTM, Icesat/GLAS, and field data. Height model is extracted from ALOS PALSAR,

X SAR, and Icesat/GLAS. The focus area is in yellow box, see Figure 2-1.

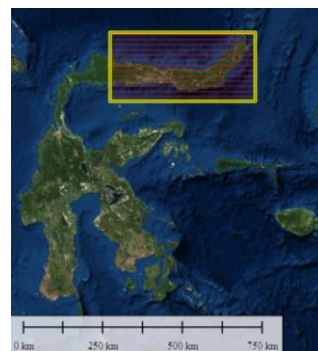


Figure 2-1: Northern of Inverse Arc Sulawesi in yellow box

The detection of this energy and mineral resources potential requires several stages: (a) mining land identification, (b) geological parameter extraction, (c) preparation of standardized spatial data with re-classed and analyzed using Geographic Information System (GIS) between each geological parameters, and (d) geothermal manifestation using physical geodesy approach in Barthelmes method, presented in Figure 2-2.

The detail stages are as follows: (a) The identification of mining land and its changes using Vegetation Index Differencing (VIDN) methods (Julzarika, 2018b). This step use Landsat data.

VIDN represents a reduction of two NDVI vegetation indexes (Nielsen, 2010; Julzarika, 2018b). VIDN values will range from -2 to 2 (Prasad & Prabhu, 2011). Negative values suggest a reduction in biomass or green vegetation and an indication of land cover change (Tjahjaningsih *et al.*, 2015). From each selected synthetic image, then a threshold is made to determine the open area of the mine (Julzarika, 2018a). The upper threshold (T_u) and lower threshold (T_d) values of each threshold are determined based on the sample pixel value in the ex-mining area (Liu *et al.*, 2013; Schölkopf *et al.*, 1998).

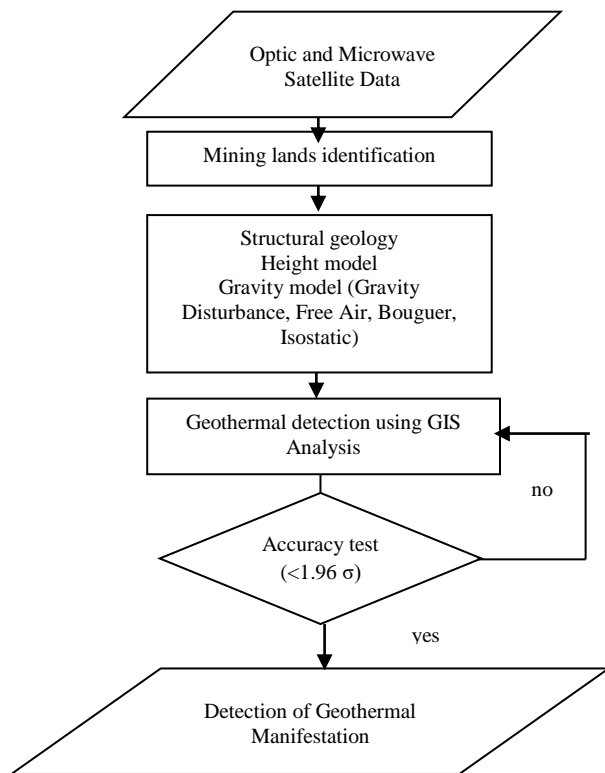


Figure 2-2: flowchart of geothermal manifestation potential

(b) Geological parameters extracted are structural geology, height model, and gravity model. The detection of these structural geology uses dip and strike methods (Rajendran *et al.*, 2013; Julzarika, *et al.*, 2013). Height model is made by using various Digital Surface Model (DSM) integration methods

(Julzarika, 2015). DSM is made from SAR data by using interferometry method.

(c) The preparation of standardized spatial data. The spatial data include raster (mining lands identification, height model, and gravity model) and vector (structural geology). Both of them must be standardized or reclassified. The raster data must have valid statistics. Calculated statistics can be used for making valid statistics.

To make standardized spatial data, the range should not overlap except at the boundary of three input raster data ranges. The range must be re-classed. Each re-classed must be set to a certain standard. The number and width of the range must be equaled for each map layers. .

For example, the mining lands re-classed, mining lands class to value 1 and non mining lands class to value 0. if ranges of height model and gravity model are specified, such as reclassifying values 0 to 100 m ; 0 to 100 miliGals (mGals) as 1 and values 100 to 300 m ; 100-200 mGals as 2, an input value less than or equal to 0 m; 0 mGals will be assigned the value 1 in the output, and an input value that is larger than 100 m, such as 100.01 m, will be assigned to 2.

After the remapping, the reclassification table has been modified. The table will not be updated if new raster are selected. The reclassification is not suitable for the new raster; a new reclassification can be reinitialized.

Structural geology is defined to identify potential reclassification results along the structural lines.

(d) Geothermal manifestation are an indication of geothermal potential. To produce the geothermal manifestation, the physical geodesy methods implemented is Barthelmes approach (Barthelmes, 2014). The gravity of the

earth is analyzed using physical geodesy approach. Barthelmes is one of the methods used in physical geodesy approach.

Gravity model include free air, gravity disturbance, Bouguer, and isostatics (Hirt *et al.*, 2012). The harmonic expansion coefficient of spherical gravitational field is the parameter for gravitational potential. Disturbing potential is obtained by reducing the gravitational potential of the reference ellipsoid (Barthelmes and Kohler, 2012). Spherical harmonic coefficients of the ellipsoid reference differ from zero to $n = 0, 2, 4, \dots$ and $l = 0$, and are calculated to degrees $n = 20$ (Bucha and Janak, 2013). The spherical harmonic coefficients of the reference ellipsoid are correctly adjusted to the values of GM and R of a given global gravity model (Barthelmes, 2013).

Gravity disturbance defined as: given the gravitational potential of topography $Q(r, \vartheta, \lambda)$, expressed in spherical harmonic expansion, the topographic effect is calculated by: (Barthelmes, 2014)

$$\delta g(r, \vartheta, \lambda) = -\frac{\partial T(r, \vartheta, \lambda)}{\partial r} \quad (2-1)$$

$$= \frac{GM}{r^2} \sum_{n=0}^N \sum_{l=0}^n \left(\frac{a}{r}\right)^n (n+1) (\Delta C_{nl} \cos l\lambda + \Delta S_{nl} \sin l\lambda) P_{nl}(\cos \vartheta)$$

$C_{nl}^{Topo}, S_{nl}^{Topo}$: The coefficient of the spherical harmonic expansion model. This coefficient is from the potential gravity of the topographic mass.

The Bouguer field is defined by:

$$\delta g_{BG}(r, \vartheta, \lambda) = \delta g(r, \vartheta, \lambda) - \delta g_{topo}(r, \vartheta, \lambda) \quad (2-2)$$

For illustrations from Figure 2-3 of heat flow variations (black isolates in mW / sqm, inferred from Cataldi, 1995) include Bouguer anomalies. The highest heat current is found in the volcano, which correlates well with the positive Bouguer value and reflects the thinning crust. Low Bouguer values in the center of ground point (Po) plains do not reflect thickening of the crust, due to the low and flat topography of the center of ground point plateau, but sub-surface density variations, which can be better identified in gravity disturbance.

The Bouguer field is calculated through a global model expressed in the spherical harmonic expansion of the observed gravitational field and the gravitational field generated from topographic and bathymetric masses. (Claessens and Hirt, 2013; Hirt and Kuhn, 2012).

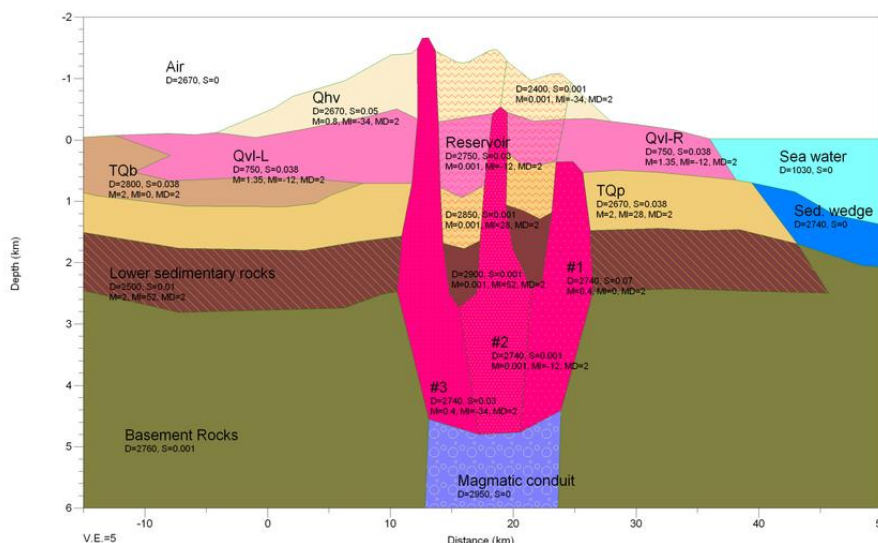


Figure 2-3: Geothermal reservoirs (Cataldi, 1995)

This geothermal manifestation on its geospatial information and geological parameters use a scale of 1: 50,000 with reference to ASPRS Accuracy Data for Digital Geospatial Data (ASPRS, 2014).

3 RESULT AND DISCUSSION

The results of the final research are information on geothermal manifestations in the Northern inverse arc Sulawesi. The detailed results are divided into steps 1-4. The result of the first step is the detection of mining lands using the VIDN method, see Figure 3-1.

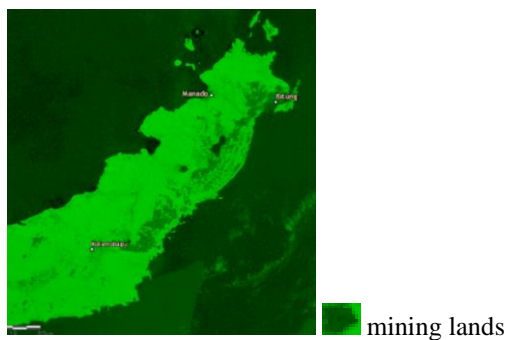


Figure 3-1: Mining lands identification

In this area, only a few mining lands are found. This is because the image used is still in medium spatial resolution. Mining land in this region is still on a small scale. This condition has no significant effect on the detection of geothermal manifestations. This

resulted in the geological parameters being more dominant in detecting geothermal manifestations. The next process is the extraction of geological parameters in step 2.

The result of the second step are Figure 3-2, 3-3, and 3-4. Earth gravity has four parameters that can be used for the extraction of energy potential and mineral resources, namely gravity disturbance, isostatic, free air, and Bouguer. Gravity disturbance is the difference between the measured gravity at a ground point and normal gravity at the same point, whereas gravity anomaly is the difference between the gravity observed in ground point, and the normal gravity in geoid, the point at which normal to the ellipsoid at ground point cuts the geoid. Isostatic can be calculated that the observed deflection can be explained if the mass of the excess mountain is matched to the same mass deficiency beneath it. Mountains are in isostatic equilibrium (isostatic equilibrium).

Free-air anomalies are calculated by correcting observations for expected variations due to spheroid and elevation above sea level. Bouguer is used to calculate the rock thickness between observation and sea level.

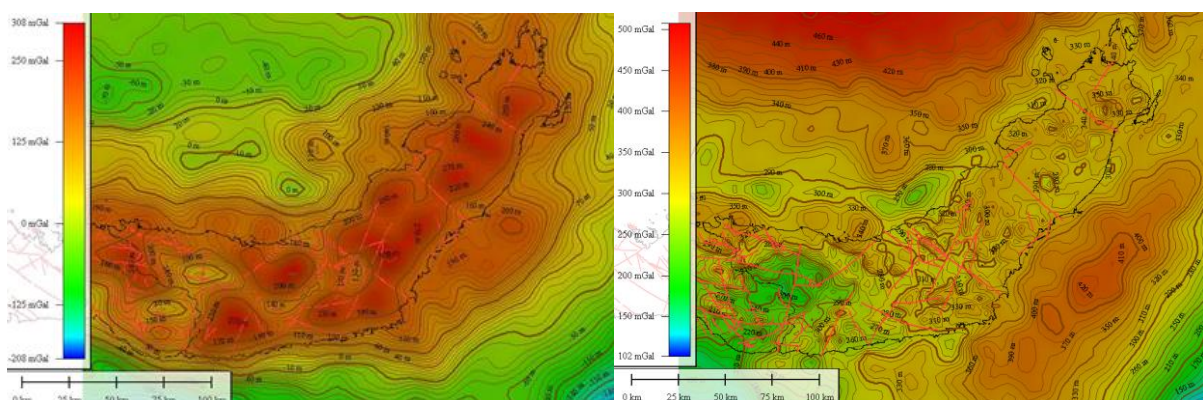


Figure 3-2: free air (left) in mgal units (yellow: high and blue values: low values) and free air are indicated by contour line, Bouguer (right)

The gravity anomalies mapped are free air and Bouguer. The free air map provides information on geological structures while the Bouguer map uses Geodesy satellite data such as GOCE with topography to show the difference in the thickness of the earth's crust. When combined these two parameters, it can be obtained a clear picture of the location of geothermal reservoirs.

The boundary between different rock types produces the permeable geometry that forms the path. An important component to exploit geothermal energy is the presence of heat in the upper layers of the earth's crust and the means to direct it to the surface.

Exploration of geothermal energy depends on access to increased surface subsurface temperatures. The crust temperature is governed by the heat fluxes of the hot coat and by the production of heat by radioactive decay in the Earth's crust. The thin crust carries a warmer coat near the surface. Therefore, increasing temperatures are found at shallow depths. A magmatic intrusion of hot gasses and hot liquid rock causes it to slowly cool down in the earth's crust. In orogens the natural radioactivity of rocks generates heat, resulting in a rise in heat and regardless of the existing coat. To bring heat to the surface, water is the transport medium. The solid rock is too compact to have the hot liquid reach the surface, so the permeable path must be found.

Heat measurements in the earth's crust are time-consuming tasks that require indirect investigation methods that can be used on a large scale, such as with remote sensing or physical geodesy from satellites. The gravitational field from Grace and GOCE satellites is a new investigation spatial tool for large-scale mapping. Bouguer maps and free water maps provide

complete information. In general, thicker crust yields a more negative Bouguer value while the thinner crust has a more positive Bouguer value. This is particularly evident in the high Bouguer values of the oceans and the negative Bouguer values for mountain ranges.

The free-air field parameter is used for geological structure mapping. This parameter can be determined its boundaries of separate rock types. The prospect of geothermal sources is very time consuming and should be focused on limited areas that have a high probability of being exploited. Gravity maps from Grace and GOCE can be integrated with hot flow values and hot flow maps. Gravity maps can be possible to become a medium of global probability classification. It is especially useful in areas where there is no local gravity and seismic data. Once a potential area has been identified, the next step is a local survey involving high resolution measurements and detailed inquiry.

Figure 3-2 illustrates the gravity values extracted from satellite data in mGals. Gravity is used to calculate the density of the energy mineral resources potential. Meanwhile, the magnetic field affects both vertical deformation and horizontal deformation occurring at locations detected in early energy mineral resources potential. Red and yellow color indicates higher value of gravity. Green color indicates medium value of gravity. Green and blue color indicates lower value of gravity. The structural geology in Figure 3-2 is symbolized by lines. The lines tip signifies the direction of the structural geology, while the line signifies the gravity disturbance field potential that occurs in the region. It uses formula (2-1).

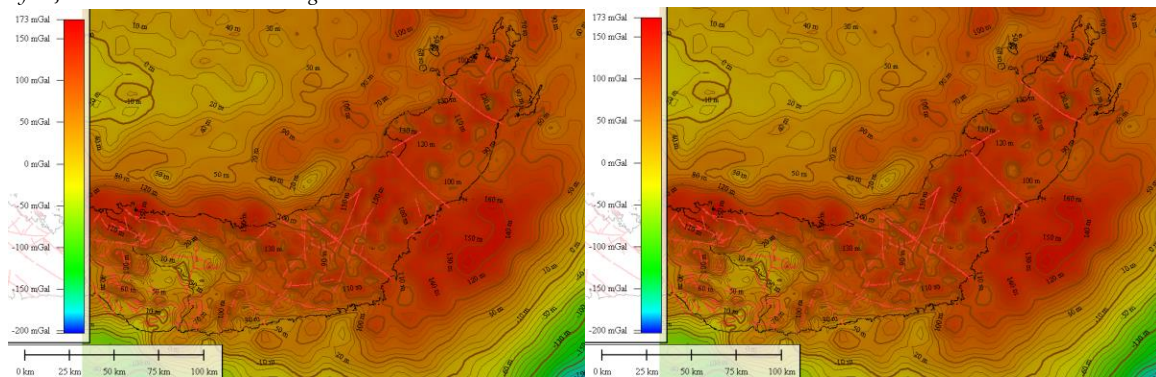


Figure 3-3: gravity disturbance (left) and isostatic (right), structural geology in red lines

Height model is required for various applications, such as for the detection of structural geology. This height model integration generates DSM so that terrain correction and height error correction is required. It aims to transform DSM into DEM and DTM as well as increase the value of its vertical accuracy. The height model integration in Figure 9 is a height integration model with a vertical accuracy of ± 1.5 m.

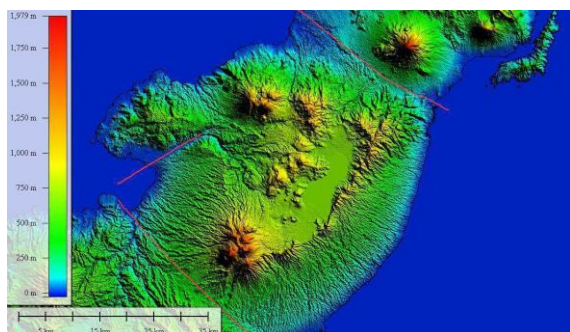


Figure 3-4: Height Model Integration (red, yellow, and green: topography with vertical accuracy 1.5 m)

The effects of topographic gravity should be calculated at the same height as gravity impairment, to the same degree and sequence and reduced. To reduce these effects, it uses the height model integration. The reduction density for topography and oceans are 2670 kg/m^3 and 1030 kg/m^3 , respectively. If the Bouguer grid is used for forwarding or inverting the density anomalies in the crust or mantle, care should be taken to use an 8000m

height calculation above the GRS80 ellipsoid. Overlay the value of heat flow on measurement point on the gravity disturbance map. Low gravity disturbances (low values) across the gravity point valley and correlate very well with low heat flow rates.

All parameters that have been extracted based raster and vector data are re-classed and analyzed using the GIS method. Result third step is Table 3-1.

Table 3-1: An example of re-classed data preparation for step 4 (combination of data factors)

Old Values	New Values
0 - 100 m	1
100 - 300 m	2
300 - 700 m	3
700 - 1200 m	4
1200 - 2000 m	5
NoData	Nodata

Table 3-1 is an example of a re-classed data for the preparation of standard spatial data. Each raster data includes identification of mine lands, height model, and gravity model performed by the re-classed. Then spatial analysis is carried out on geological structure data. Standardized spatial data aim to ease in spatial data analysis and use least memory of computer in processing.

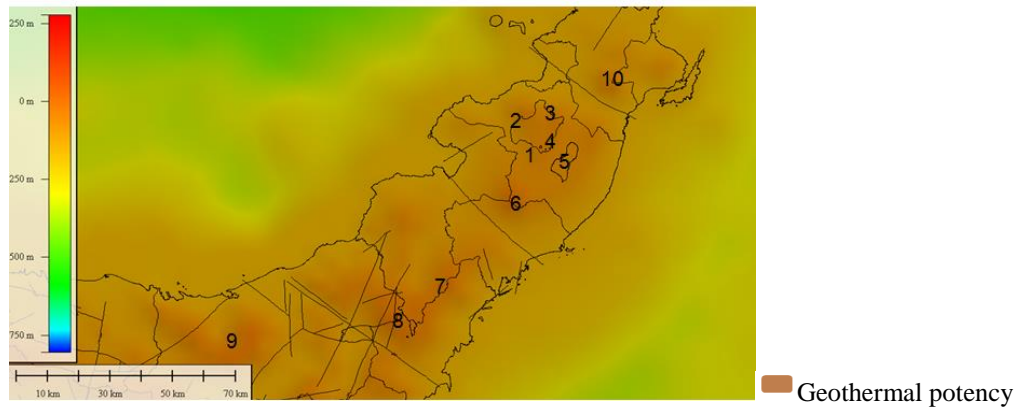










Figure 3-5: Potential of geothermal manifestation identification results using remote sensing (no 1 to 10), they are overlay into gravity disturbance imagery.

Table 3-2: Accuracy test by comparing detection results from remote sensing with the field.

ID	Photo	Result	ID	Photo	Result
ST 1		Found manifestations of hot springs	ST 6		Found manifestation of fumaroles
ST 2		Found manifestation of fumaroles	ST 7		Found manifestation of fumaroles
ST 3		Found manifestation of fumaroles	ST 8		Found manifestation of fumaroles
ST 4		Found manifestation of fumaroles	ST 9	-	Not enough time for ground validation
ST 5		Not found manifestation	ST 10	-	Not enough time for ground validation

The result of the fourth step is presented in Figure 11. Based on the results of the analysis from the result of the third step and physical geodesy method in step 4, there are 10 locations that have potential geothermal manifestations. These locations are

scattered to follow a series of volcanoes along the Sulawesi Inverse Arc. All of these locations require checking in the field whether geothermal manifestations are found or only blunders on the count of gravity anomalies. This field check uses an accuracy test.

Accuracy test

The accuracy test includes 10 test points, can be seen in Table 3-2. After the field test of 10 potential points of geothermal manifestation, it resulted that there are 7 points found to be the potential manifestations of fumaroles, hot springs, and crater of the mountain. One point has not yet been found for potential geothermal manifestations. Two locations were not checked because there was not enough survey time. The accuracy of this study was 87.5% with a confidence level of 1.96σ . In ST 1, geothermal manifestations in the form of hot springs were found. This location is located around the state electricity company of Lahendong area. In ST 2, geothermal manifestations in the form of Fumaroles were found. The location is in the pine forest of Lahendong. The location of ST 3 is located at the top of Mount Mahawu. In the crater of the mountain, there were Fumaroles found dried up. Then on ST 4, active fumaroles were found. The location of ST 4 is at Lake Linow Lahendong. Fumaroles are spread along the west-north-east side. Lake water is also hot and contains sulfur with the appearance of green water.

The location of ST 5 is on Lake Tondano. After checking in the field, geothermal manifestations have not been found. If this location is a geothermal potential, the manifestation might be in the bottom of lake or in the lake subsurface. In ST 6, geothermal manifestations of fumaroles were found. Location ST 6 is at the Mount Soputan. The locations of ST 7 and ST 8 are on a mountain near Lake Moat, Kotamobagu. At these two locations, geothermal manifestations of fumaroles were found. The locations of ST 9 and ST 10 are around North Minahasa and Bitung. During the field survey there was not

enough time to conduct checking and validation.

4 CONCLUSIONS

Remote sensing can be used to detect potential geothermal manifestations. There are four steps to detect geothermal manifestation, namely (a) mining land identification, (b) geological parameter extraction, (c) preparation of standardized spatial data, and (d) geothermal manifestation.

Detection results with remote sensing are 10 potential geothermal manifestations. After the field test, it is found that there are 7 points having the potential manifestations of fumaroles, hot springs, and crater of the mountain. There are two points are not checked due to not enough time. One point has not yet been manifested. The accuracy of this study was 87.5% with a confidence level of 1.96σ . This research still needs further study, namely by connecting it to geoelectric parameters, density, and geodynamics.

ACKNOWLEDGEMENT

Author would like to thank LAPAN, Gadjah Mada University (UGM), PT. Pertamina Geothermal Energy (PT. PGE), DLR, USGS, Alaska University, and ESA for the success of this research in 2017. Special thanks to ESDM team of LAPAN 2017.

REFERENCES

- ASPRS. (2014). ASPRS Accuracy Standard for Digital Geospatial Data. ASPRS. United States of America.
- Barthelmes, F., (2013). Definition of Functionals of the Geopotential and Their Calculation from Spherical Harmonic Models: Theory and formulas used by the calculation service of the International Centre for Global Earth Models (ICGEM); <http://icgem.gfz-potsdam.de/ICGEM/>. Scientific Technical Report STR09/02, Revised

- Edition, January 2013, Geo Forschung Zentrum Potsdam, DOI 10.2312/GFZ.b103-0902-26, URL <http://doi.org/10.2312/GFZ.b1030902-26>
- Barthelmes, F., (2014). Global Models. In: Grafarend E (ed) Encyclopedia of Geodesy, Springer International Publishing, pp 1–9, DOI 10.1007/978-3-319-02370-0 43-1, URL <http://dx.doi.org/10.1007/978-3-319-02370-0 43-1>
- Barthelmes, F., Kohler, W., (2012). International Centre for Global Earth Models (ICGEM). Journal of Geodesy, The Geodesists Handbook 2012 86(10):932–934, DOI 10.1007/s00190-0120584-1, URL <http://dx.doi.org/10.1007/s00190-012-0584-1>
- Bucha, B., & Janak, J., (2013). Code and readme of a MATLAB-based graphical user interface program for computing functionals of the geopotential. PANGAEA, <https://doi.org/10.1594/PANGAEA.808577>.
- Cataldi, R., (1995). Social acceptance: a sine qua non for geothermal development in the 21st century. Bulletin d'Hydrogiologie No 17 (1999). Centre d'Hydrogtologie, Universiti de Neuchdtel, Editions Peter Lang.
- Claessens and Hirt, (2013). Ellipsoidal topographic potential: New solutions for spectral forward gravity modeling of topography with respect to a reference ellipsoid. Journal Of Geophysical Research: Solid Earth, VOL. 118, 5991–6002, doi:10.1002/2013JB010457.
- EORC JAXA, (2018). Fundamentals of Remote Sensing. JAXA. Jepang.
- Hirt, C., & M. Kuhn, (2012). Evaluation of high-degree series expansions of the topographic potential to higher-order powers, Journal Geophysical Research (JGR) - Solid Earth, in press. doi:10.1029/2012JB009492.
- Hirt, C., M. Kuhn, W.E. Featherstone & F.Goettl, (2012). Topographic/isostatic evaluation of new-generation GOCE gravity field models, Journal of Geophysical Research - Solid Earth, B05407, doi: 10.1029/2011JB008878
- Jin, H., Mountrakis, G., & Stehman, SV, (2014). Assessing Integration of Intensity, Polarimetric Scattering, Interferometric Coherence and Spatial Texture Metrics in PALSAR-Derived Land Cover Classification. ISPRS Journal of Photogrammetry and Remote Sensing, 98, 70-84.
- Julzarika, A., (2018a). Penginderaan Jauh untuk Pendeteksian Awal Potensi Tembaga Di Sumbawa. Jurnal Riset Geologi dan Pertambangan, Vol.28, No.1, Juni 2018, 75-89. ISSN 0125-9849, e-ISSN 2354-6638 Ris.Geo.Tam Vol. 28, No.1, Juni 2018 (75-89) DOI: 10.14203/risetgeotam2018.v28.434.
- Julzarika, A., (2018b). Mining land identification in Wetar Island using remote sensing data. J. Degrade. Min. Land Manage. 6(1): 1513-1518, DOI: 10.15243/jdmlm.2018.061.1513.
- Julzarika, A., Laksono, DP, Subehi, L., Dewi, EK, Kayat, Sofiyuddin, HA, & Nugraha, MFI, (2018). Comprehensive integration system of saltwater environment on Rote Island using a multidisciplinary approach. J. Degrade. Min. Land Manage. 6(1): 1553-1567, DOI: 10.15243/jdmlm.2018.061.1553.
- Julzarika, A., & Anggraini, N., (2017). Detection of Energy and Mineral Resources Potential in Efficient and Effective using Remote Sensing. Joint Convention Geology-Geophysyc, Petroleum Engineer. Malang.
- Julzarika, A., Susanto, & Sutanto, A., (2013). Pengembangan Model Standar Pemanfaatan Data Penginderaan Jauh (Optik dan SAR) untuk Identifikasi Sumber Daya Mineral Tembaga. Laporan Penelitian Inhouse Tahun 2013. LAPAN. Jakarta.

- Julzarika, A., (2015). Integration of Height Model using SRTM C, X SAR, Aster GDEM, and ALOS Palsar. Asian Conference on Remote Sensing.
- KESDM. (1999). Kepmentamben no 1519.K/20/MPE/1999. KESDM, Jakarta.
- Liu, L., Zhou, J., Yin, F., Feng, M., & Zhang, B. (2013). The reconnaissance of mineral resources through ASTER data-based image processing, interpreting and ground inspection in the Jiafushaersu area, West Junggar, Xinjiang (China). *J. Earth Science*.
- Nielsen, A., (2010). Kernel Maximum Autocorrelation Factor and Minimum Noise Fraction Transformations. *IEEE Transactions on Image Processing* (Volume20, Issue: 3, March 2011).
- Prasad, K., & Prabhu, GK, (2011). Diag-AID: A Diagnostic Aid for Medical Image Enhancement using Colour Coding and Modified Histogram Equalisation Techniques. *International Journal of Medical Engineering and Informatics*, 3(3), 223-233.
- Rajendran, S., Nasir, S., Kusky, TM, Ghulam, A., Gabr, S., & El-Ghali, MA, (2013). Detection of Hydrothermal Mineralized Zones Associated with Listwaenites in Central Oman using ASTER Data. *Ore Geology Reviews*, 53, 470-488.
- Schölkopf, B., Smola, A., & Müller, KR, (1998). Nonlinear Component Analysis as a Kernel Eigenvalue Problem. *Neural Computation*, 10(5), 1299-1319.
- Tjahjaningsih, A., Julzarika, A., Sutanto, A., & Nugroho, UC, (2015). Pemanfaatan data penginderaan jauh untuk identifikasi tambang emas di Geumpang Aceh. Laporan penelitian inhouse 2015. LAPAN. Jakarta.
- Youssef, AM, Pradhan, B., Sabtan, AA, & El-Harbi, HM, (2012). Coupling of Remote Sensing Data Aided with Field Investigations for Geological Hazards Assessment in Jazan Area, Kingdom of Saudi Arabia. *Environmental Earth Sciences*, 65(1), 119-130.
- Zhou, J., Liu, L., Jiang, D., Zhuang, D., Mansaray LR, & Zhang B., (2013). Targeting Mineral Resources with Remote Sensing and Field Data in the Xiemisitai Area, West Junggar, Xinjiang, China. *Journal Remote Sensing*, 5(7), 3156-3171.